Journal of Fluids and Structures (2001) **15,** 1123–1135
doi:10.1006/jfls.2001.0394, available online at http://www.idealibrary.com on IDEAL®

FLOW CHARACTERISTICS AROUND AN INCLINED ELLIPTIC CYLINDER IN A TURBULENT BOUNDARY LAYER

J.H. Choi and S.J. Lee

Department of Mechanical Engineering, Pohang University of Science & Technology Pohang 790-784, Korea

(Received 7 June 2000, and in final form 4 December 2000)

The flow characteristics around an inclined elliptic cylinder located near a flat plate were investigated experimentally. The axis ratio of the elliptic cylinder was AR = 2. The pressure distributions along the surface of the cylinder and the flat plate were measured by varying the angle of attack of the elliptic cylinder. The velocity profiles behind the cylinder were measured using hot-wire anemometry. When the angle of attack varies, the peak pressure location on the windward cylinder surface moves towards the rear edge of the cylinder, while that on the leeward surface moves towards the front edge of the cylinder. The vortex-shedding frequency also gradually decreases, defining a critical angle of attack for each gap ratio. The location of the minimum pressure on the flat plate surface moves downstream for positive angles of attack, while it moves upstream for negative angles of attack. Negative angles of attack cause a greater disturbance in the boundary layer near the wall compared to positive angles of attack. This shows that the separated wall shear layer from the boundary layer and the lower shear layer of the cylinder wake are strongly merged compared to other cases.

1. INTRODUCTION

Flow characteristics around a bluff body immersed in a boundary layer have been widely investigated, both for academic interest and for a wide range of practical applications. This kind of flow can be observed in many engineering problems, such as undersea pipelines, multi-element airfoils and heat exchangers. There are many previous studies on the flow around a bluff body of various shapes located near a flat plate.

Zhou & Squire (1985) investigated the flow around an airfoil placed near a wall. They found that the level of turbulence has a large effect on the interaction between the boundary layer and airfoil of various shapes. Ranzenbach & Barlow (1994) investigated the flow characteristics around a NACA 0015 airfoil placed at various heights above the ground. They found that as the height decreases, a negative lift force exists on the airfoil until a critical height, below which the lift force becomes positive. They showed that this lift force reversal is related to the merging of the airfoil wake and plane boundary layer.

Marumo *et al.* (1978) investigated the boundary layer disturbed by a circular cylinder for various gap ratios. They found that the boundary layer recovers faster in the inner (near the plate) region than in the outer region and the velocity fluctuations recover faster than the mean velocity components.

Bearman & Zdravkovich (1978) measured the vortex structure and pressure distribution along a circular cylinder embedded in a boundary layer whose thickness was 0·8 times the cylinder diameter. They found that vortex shedding is restricted for gap ratios less than the critical gap ratio of 0·3. However, the Strouhal number St remains nearly unchanged for gap

0889–9746/01/081123 + 13 $35.00/0

ratios greater than the critical gap ratio. Lei *et al.* (1999) studied the effect of a plane boundary layer on the aerodynamic forces and vortex shedding of a circular cylinder near the wall. They found that the aerodynamic forces acting on the cylinder are more dependent on the gap ratio than on the thickness of the boundary layer. The critical gap ratio decreases slightly as the boundary layer thickness increases. However, the Strouhal number does not change significantly with either the gap ratio or the boundary layer thickness.

Choi & Lee (2000) investigated the flow characteristics around an elliptic cylinder immersed in a thick turbulent boundary layer. The vortex-shedding frequency of the elliptic cylinder decreases on decreasing the gap ratio. They also found that the critical gap ratio is larger than that of a circular cylinder with the same vertical height.

From a practical point of view, an airfoil-shaped bluff body such as an elliptic cylinder at incidence has wide engineering applications. The flow structures around an elliptic cylinder located in a uniform flow become altered considerably depending on the axes ratio and the angle of attack of the cylinder (Modi & Wiland 1970; Modi & Dikshit 1975). The drag coefficient of an elliptic cylinder in a uniform flow with small angle of attack is much lower than that of a circular cylinder. The heat transfer coefficient of the elliptic cylinder was found to be nearly equal to or a little higher than that of a circular cylinder (Ota *et al.* 1984, 1987).

In most previous studies, a bluff body such as an airfoil or noncircular cylinder was submerged in a boundary layer parallel to a flat plate at a zero angle of attack. Therefore, the interaction between the wake behind a bluff body at incidence and the boundary layer has not been fully investigated.

In this study, the flow characteristics around an inclined elliptic cylinder immersed in a thick turbulent boundary layer have been investigated experimentally for various distances over the ground plate. The main objective is to understand the interaction between the boundary layer and the asymmetric wake behind the elliptic cylinder at various angles of attack.

2. EXPERIMENTAL APPARATUS AND METHODS

Experiments were performed in a subsonic wind tunnel with a test-section that was 0·6 m in height, 0·72 m in width and 6 m in length. The free-stream turbulence intensity in the test-section was less than 0·08% at 10 m/s. Figure 1 shows the geometric shape of the elliptic cylinder and a schematic diagram of the experimental setup. An elliptic cylinder with an axis ratio ($AR = A/B$) of $AR = 2$ and length of 600 mm was used in this study. Here, A and B are the radii of the major and minor axes of the elliptic cylinder.

A smooth flat plate with a thickness of 15 mm and a length of 4·8 m was installed 100 mm above the bottom surface of the test-section. The leading edge of the plate was sharp-edged with an angle of 30°. The elliptic cylinder was placed 1·5 m downstream from the leading edge of the flat plate. At each end of the elliptic cylinder, a rectangular end-plate was attached to maintain two-dimensional flow characteristics in the cylinder wake by minimizing the effect of the boundary layer developed along the wind tunnel side-wall. A trip wire with a diameter of 3·5 mm was attached to the flat plate, 100 mm downstream from the leading edge, to generate a thick turbulent boundary layer. During the experiment, the free-stream velocity (U_0) was fixed at 10 m/s and the boundary layer thickness formed over the flat plate was $\delta = 75$ mm at the cylinder location. The Reynolds numbers based on the height (B) of the elliptic cylinder and the boundary layer thickness (δ) were $Re_B = 13\,600$ and $Re_\delta = 48\,000$, respectively.

The variable H is the distance between the center of the cylinder and the flat plate. The angle of attack of the elliptic cylinder, α, has positive values on clockwise rotation. The

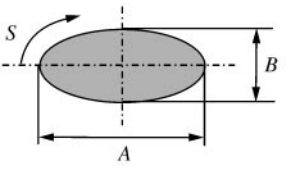

AR (A/B)	A (Major axis)	B (Minor axis)
2	42·4	21·2

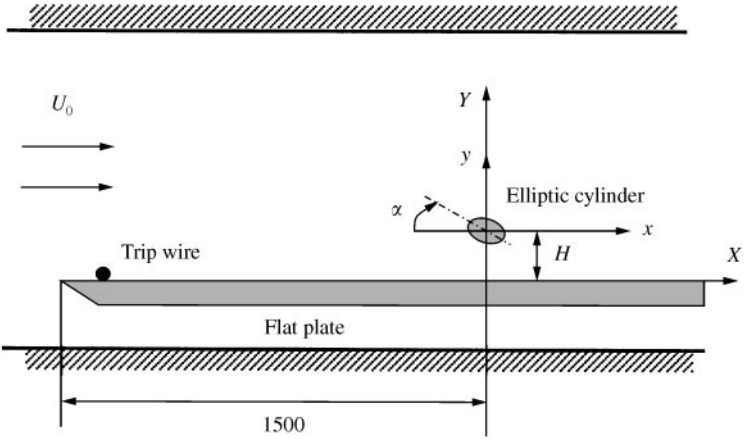

Figure 1. Schematic diagram of experimental setup and geometric shape of the elliptic cylinder used in this study (dimensions in mm).

origin of the absolute coordinates (X, Y) is at that point where the vertical centerline of the cylinder intersects with the flat plate. The absolute coordinates X and Y give the streamwise and vertical distances from the origin, respectively. The relative coordinates x and y indicate the corresponding relative distances from the center of the cylinder.

To measure pressure distributions along the cylinder surface and flat plate, pressure taps, 0·8 mm in diameter, were installed at regular intervals. The pressure taps were connected to the Scannivalve (48J9-1), and analog pressure signals were digitized using a high-precision A/D converter (DT 2838). The pressure difference between the surface pressure P_s and the reference pressure P_0 measured at ambient free stream was nondimensionalized using the dynamic pressure at the free stream velocity U_0. The pressure coefficient C_p and lift coefficient C_L were expressed as follows:

$$C_p = \frac{P_s - P_0}{\rho U_0^2/2}, \qquad C_L = \frac{L}{\rho U_0^2 A/2}.$$

Here, A denotes the length of the major axis of the cylinder.

The lift force (L) acting on the cylinder was numerically calculated from the surface pressure distribution as follows:

$$L = -\oint_S (P_s - P_0) \sin\theta \, \mathrm{d}S,$$

where, S denotes the surface distance from the leading edge of the cylinder as shown in Figure 1, and θ denotes the angle between the normal vector on the cylinder surface and free stream. The angle θ is changed with respect to the angle of attack.

Velocity profiles were measured using a hot-wire anemometer (TSI IFA 100) with I-type (DANTEC 55P11) and X-type (DANTEC 55P61) probes. In addition, a spectral analysis was performed for the measured velocity signals to investigate the interaction between the cylinder wake and the boundary layer. The X-type hot-wire probe was calibrated using the effective yaw calibration method. The hot-wire probe was traversed to the measuring points using a 3-D traversing system with an accuracy of 0·01 mm. During experiments, the temperature variation in the wind tunnel test-section was less than 0·5°C. Since the blockage ratio was less than 5%, a blockage correction on the pressure and velocity measurements was not carried out in this study (Maskell 1963).

Flow visualization was performed using a particle tracer technique to observe the flow interaction between the elliptic cylinder wake and the boundary layer qualitatively. This experiment was carried out in a circulating water channel with a test-section of $0{\cdot}3\ W \times 0{\cdot}25\ H \times 1{\cdot}2\ L$ (m^3) at the free-stream velocity of 0·2 m/s. A trip wire with 9 mm diameter and roughness elements was used to generate the same boundary layer thickness at the cylinder location. The Reynolds number in the visualization experiments was about 1/5 of its counterpart in air flow experiments. Even though the Reynolds number did not match the wind tunnel experiments exactly, the flow visualization results gave useful information to understand the flow structure qualitatively. A laser beam from a 4W Ar-ion laser was passed through mirrors and a cylindrical lens to form a thin laser light sheet, which illuminated the central streamwise cross-section. Particles (Vestosint 1111) with an average diameter of 100 μm and a specific gravity of 1·016 were seeded as tracer particles. Flow images were captured using a CCD camera (VDS CCD-1010) with a resolution of $1\ K \times 1\ K$ pixels.

3. RESULTS AND DISCUSSION

Figures 2 and 3 show some typical visualized flows around an $AR = 2$ elliptic cylinder with angles of attack $\alpha = 0$ and $\pm 15°$. For the gap ratio between the cylinder and plate of $H/B = 0{\cdot}7$, we can observe the recirculation regions in the front and rear of the cylinder, regardless of the angle of attack. At a positive angle of attack ($\alpha = 15°$), the recirculation region formed in front of the cylinder marked as a hollow arrow is larger and the extent of the recirculation region behind the cylinder marked as a solid arrow is smaller, compared to the case of zero angle of attack. On the other hand, at a negative angle of attack ($\alpha = -15°$), the recirculation region in front of the cylinder is much smaller and the recirculation region behind the cylinder is much larger, compared to the case of zero angle of attack.

For the gap ratio of $H/B = 1{\cdot}5$, we can observe the flow interaction between the boundary layer and the cylinder wake. As the flow travels downstream, vortex ejection events occur in the boundary layer behind the arrow mark, irrespective of the angle of attack. At a negative angle of attack ($\alpha = -15°$), the vortex ejection becomes weak, because the separated wall shear layer from the flat plate and the lower shear layer of the cylinder wake are strongly merged compared to other cases.

Figures 4 and 5 represent the pressure distributions along the elliptic cylinder surface as a function of the angle of attack. Here, the abscissa S denotes the surface distance from the leading edge of the cylinder; positive values indicate the distance along the upper surface as shown in Figure 1. At a positive angle of attack, the pressure distribution on the lower surface of the cylinder indicates the windward surface pressure; at a negative angle of attack, the lower surface gives the leeward surface pressure.

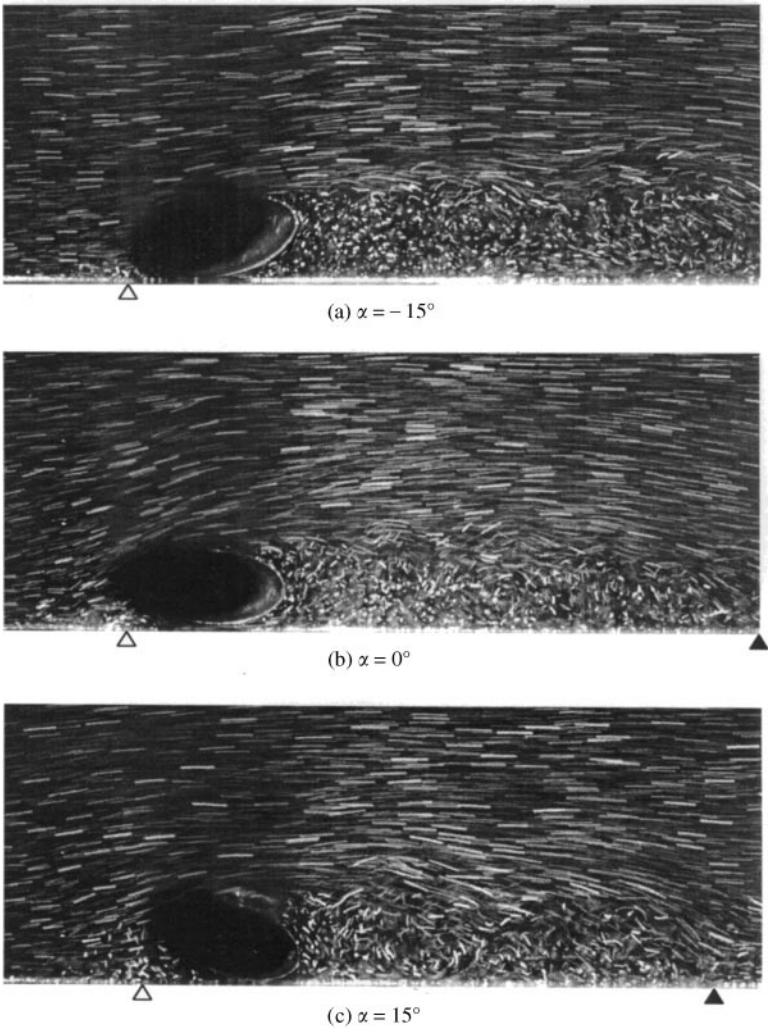

Figure 2. Flow visualization around an elliptic cylinder at $H/B = 0{\cdot}7$. $\alpha = -15^{\circ}$, $\alpha = 0^{\circ}$, $\alpha = 15^{\circ}$.

At a zero angle of attack, the lower and upper surface pressure distributions become symmetric with respect to the chord of the elliptic cylinder, as the gap ratio between the cylinder and plate increases. The location of the minimum pressure on the lower surface shifts toward the rear of the cylinder on decreasing the gap ratio, because the separation point moves downstream due to the gap flow. The effect of the gap ratio on the surface pressure distributions is noticeable on the lower surface of the cylinder as explained in the previous research (Choi & Lee 2000). This indicates that the effect of the gap flow, which affects the lower surface directly, becomes weak as the gap ratio increases.

As the angle of attack increases, the stagnation point, where the surface pressure has the maximum value, shifts downstream on the windward surface. The position of the minimum pressure on the windward surface moves towards the rear edge of the cylinder, while that of the leeward surface moves toward the front edge of the cylinder. The minimum pressure on the windward surface has a nearly constant value, regardless of the angle of attack. However, the magnitude of the minimum pressure on the leeward surface decreases as the

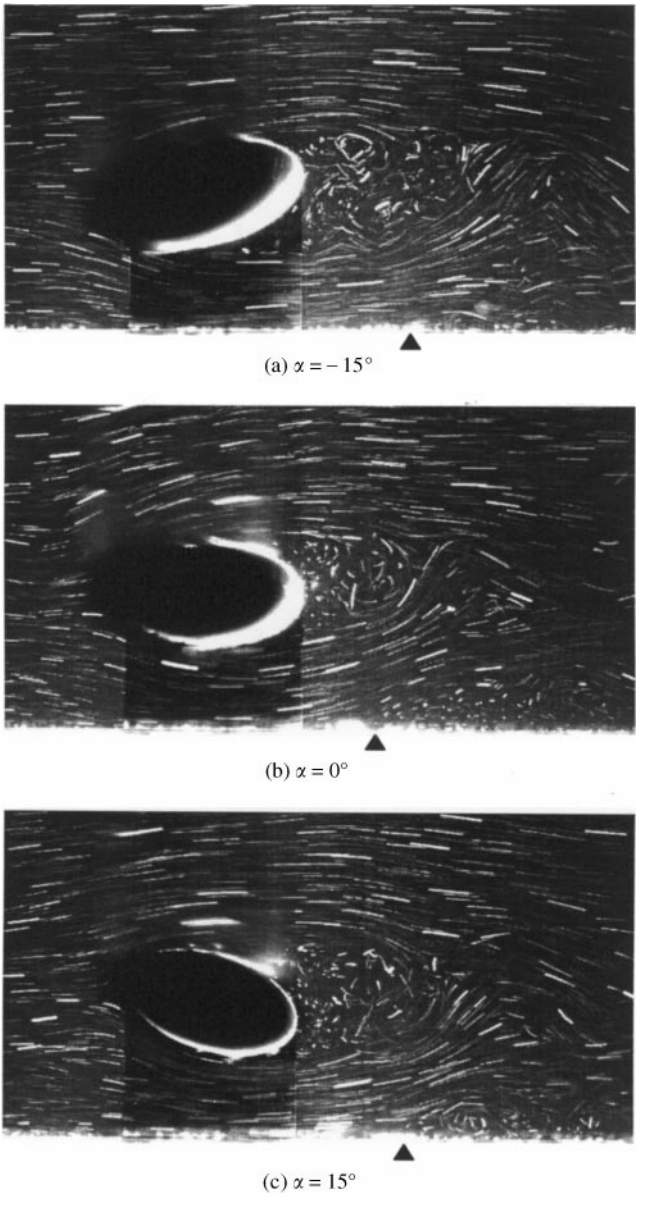

Figure 3. Flow visualization around an elliptic cylinder at $H/B = 1{\cdot}5$. $\alpha = -15°$, $\alpha = 0°$, $\alpha = 15°$.

angle of attack increases. These results agree well with those obtained from previous studies using uniform flow (Modi & Wiland 1970; Ota *et al.* 1987). At the gap ratio of $H/B = 0{\cdot}7$, the effect of the angle of attack on the pressure distribution over the cylinder surface becomes relatively large. As the angle of attack increases, the positive pressures on the windward surface increase and the negative pressures on the leeward surface decrease significantly. This seems to be caused by the choking effect of the gap flow due to the large recirculation region formed in front of the cylinder as shown in the visualized flow pattern.

At negative angles of attack, the stagnation point and the minimum pressure undergo a similar change as observed for positive angles of attack. However, as the gap ratio

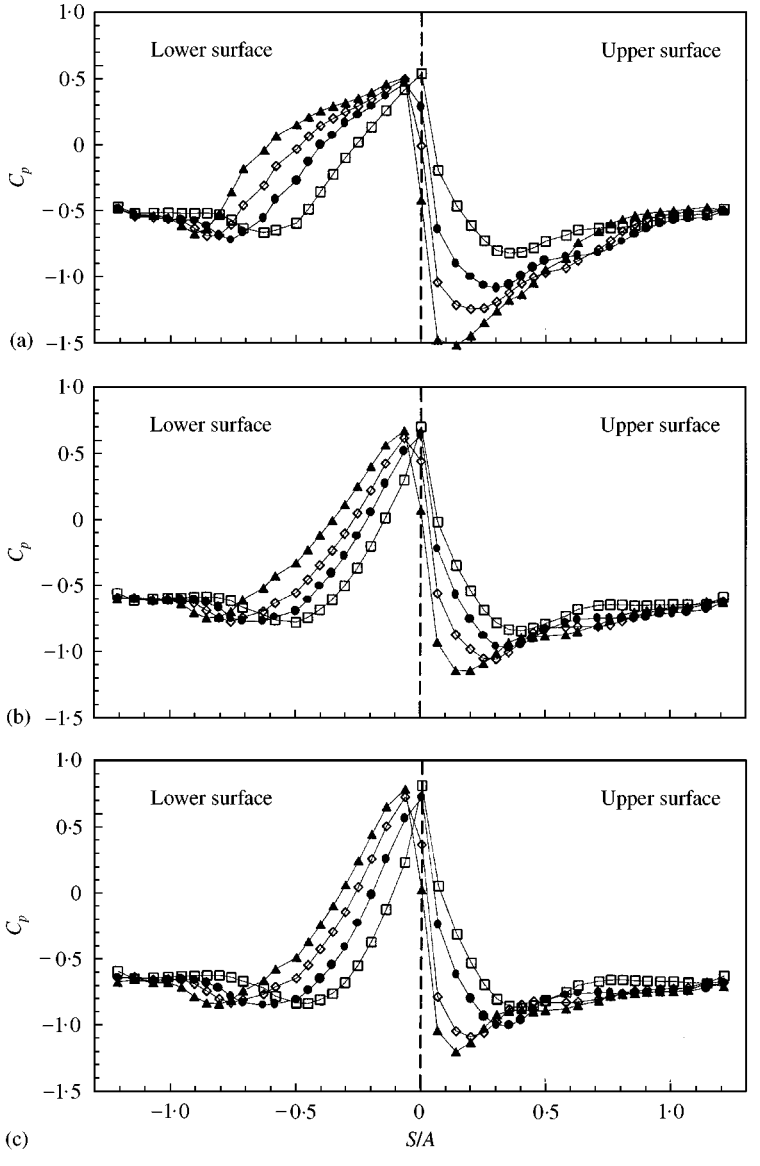

Figure 4. Surface pressure distributions on the elliptic cylinder at positive angles of attack: □, $\alpha = 0$; ●, $\alpha = 5°$; ◇, $\alpha = 10°$; ▲, $\alpha = 15°$. (a) $H/B = 0{\cdot}7$, (b) $H/B = 1$, (c) $H/B = 1{\cdot}5$.

decreases, the variation in the stagnation point decreases and the position of the minimum pressure on the lower surface moves toward the rear edge of the cylinder. For the gap ratio of $H/B = 0{\cdot}7$, the stagnation points are located at $S/A = 0{\cdot}0$ regardless of the angle of attack. This indicates that the position of the stagnation point shifts toward the flat plate due to the gap flow. At the gap ratio of $H/B = 1{\cdot}5$, the results on the lower and upper surfaces of Figure 4 correspond to those on the upper and lower surfaces of Figure 5. However, at gap ratio of $H/B = 0{\cdot}7$, the surface pressure distributions for the positive and negative angles of attack are quite different. From these results, we can see that the effect of the angle of attack becomes dominant at smaller gap ratios.

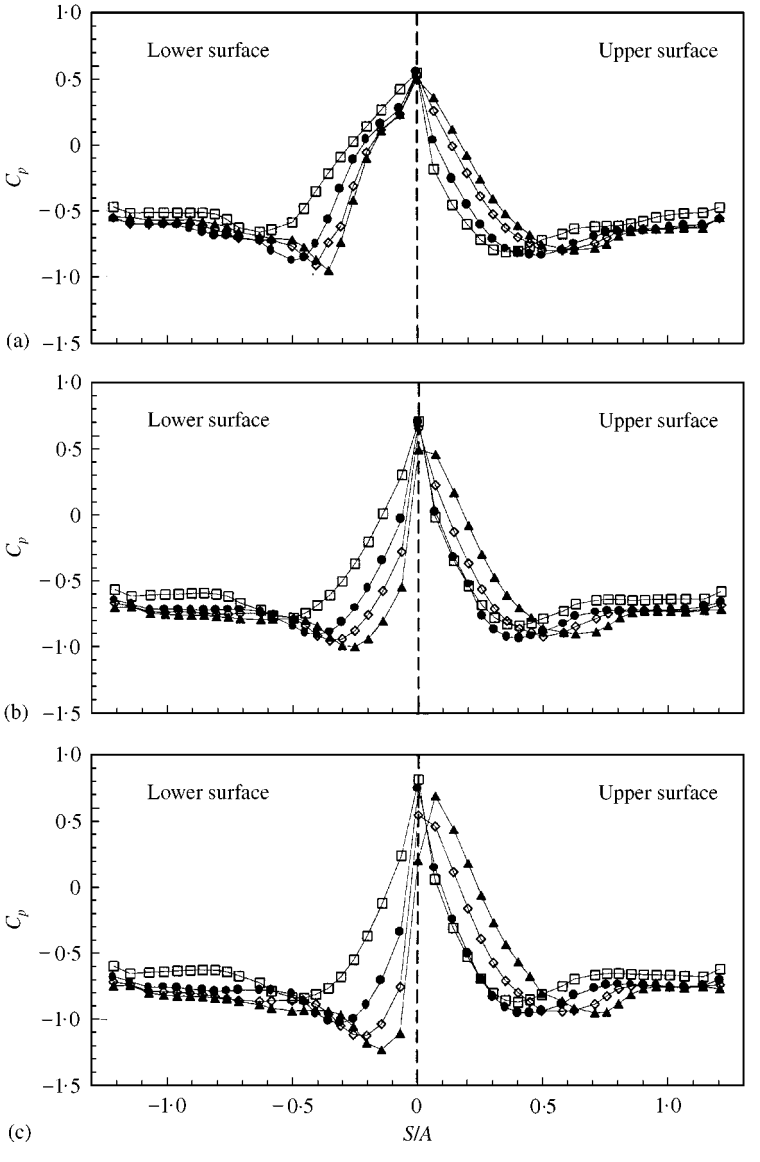

Figure 5. Surface pressure distributions on the elliptic cylinder at negative angles of attack: □, $\alpha = 0$; ●, $\alpha = 5°$; ◇, $\alpha = 10°$; ▲, $\alpha = 15°$. (a) $H/B = 0{\cdot}7$, (b) $H/B = 1$, (c) $H/B = 1{\cdot}5$.

Variations of the lift coefficient acting on the cylinder are shown in Figure 6. At a zero angle of attack, the elliptic cylinder for all gap ratios has a positive lift force due to the gap flow. As the gap ratio between the cylinder and plate increases, the lift force decreases because the pressure distribution along the cylinder surface becomes symmetric.

At positive angles of attack, the lift coefficient C_L increases with increasing angle of attack. For the gap ratio of $H/B = 0{\cdot}7$, the lift coefficient C_L increases greatly at small angles of attack between $\alpha = 0$ and 5°. This seems to be caused by the choking effect of the gap flow due to the recirculation region formed in front of the cylinder as shown in the visualized flow pattern. On the other hand, at negative angles of attack, the lift coefficient C_L becomes negative on increasing the angle of attack. As the gap ratio between the cylinder and plate

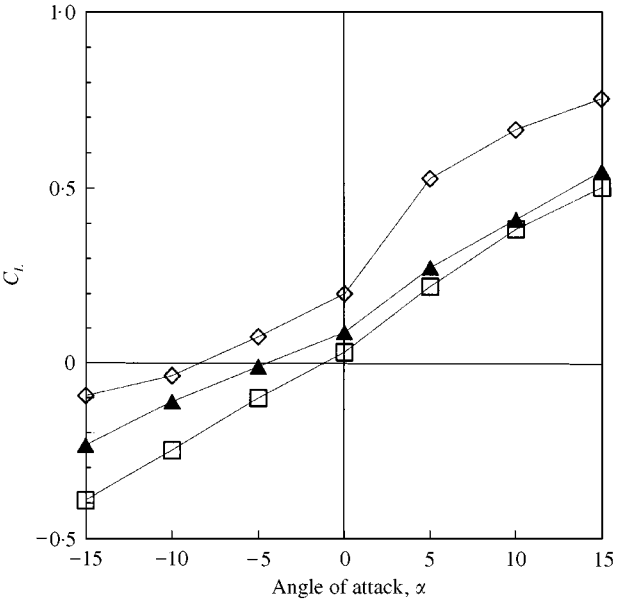

Figure 6. Variations of the lift coefficient in terms of angle of attack: ◇, $H/B = 0{\cdot}7$; ▲, $H/B = 1{\cdot}0$; □, $H/B = 1{\cdot}5$.

decreases, the lift coefficient C_L increases due to the enhanced gap flow effect, irrespective of the angle of attack. From these results, we can conjecture that the effect of the angle of attack becomes dominant at smaller gap ratios.

Figures 7 and 8 show the pressure distributions along the flat surface as a function of the angle of attack. Regardless of the angle of attack, the upstream surface pressures increase and minimum pressure decreases as the gap ratio decreases. As the flow travels downstream, the negative pressure recovers to static pressure. In addition, the location of minimum pressure moves upstream as the gap ratio decreases.

Compared to the case of zero angle of attack, the surface pressure on the flat plate increases and the minimum pressure location shifts a little downstream with increasing positive angles of attack. For the gap ratio of $H/B = 0{\cdot}7$, the recirculation region becomes smaller compared to other cases, as shown in the flow visualization result.

As the negative angle of attack increases, the minimum pressure decreases and its position shifts upstream slightly. The surface pressure on the upstream flat plate remains nearly unchanged. However, the variation in the downstream surface pressure becomes relatively large compared to the case of positive angle of attack. As the flow travels downstream, the downstream distance of the region where the negative pressure recovers to static pressure becomes larger with increasing negative angles of attack. This may be attributed to the fact that the separated wall shear layer and the lower shear layer of the cylinder wake are strongly merged. For the smaller gap ratio of $H/B = 0{\cdot}7$, the recirculation region formed behind the cylinder becomes larger than in any other cases. These results on surface pressure variation agree well with the visualized flow patterns.

In order to examine the effect of the angle of attack on the vortex structure in the near wake, the streamwise velocity fluctuations were measured using a single hot-wire probe, and a spectral analysis was carried out. The variation of the Strouhal number ($\mathrm{St} = Bf_s/U_0$) at $x/A = 1{\cdot}0$ and $y/B = \pm 0{\cdot}5$ with the angle of attack is shown in Figure 9. The Strouhal numbers measured at the y-axis have nearly the same value regardless of the measuring position. We can observe the maximum Strouhal number at a zero angle of attack and the

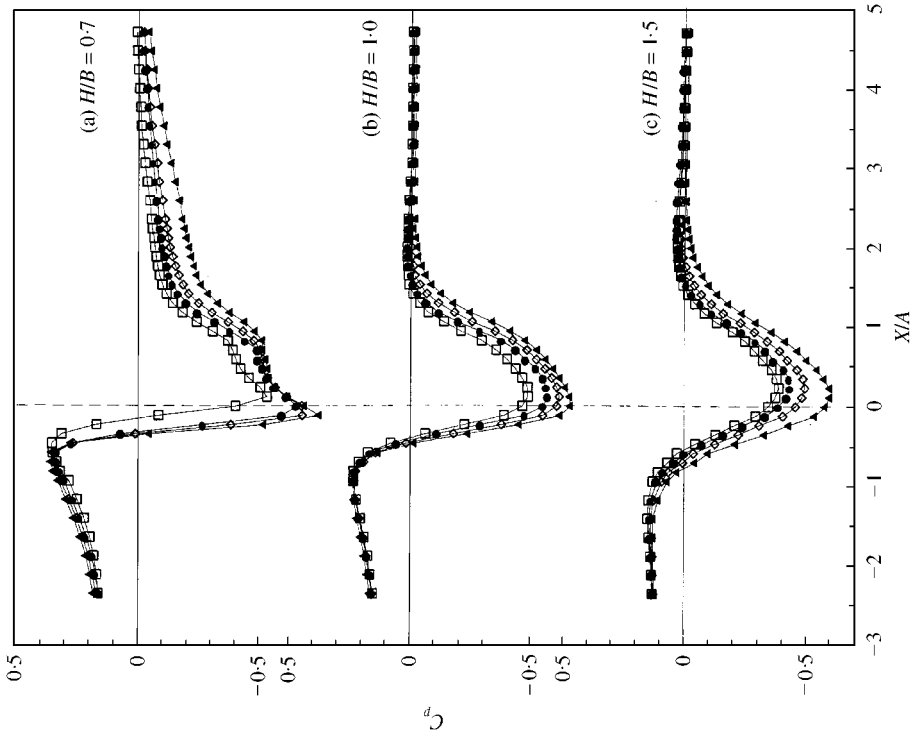

Figure 8. Surface pressure distributions on the flat plate at negative angles of attack: □, $\alpha = 0$; ●, $\alpha = -5°$; ◇, $\alpha = -10°$; ▲, $\alpha = -15°$. (a) $H/B = 0{\cdot}7$, (b) $H/B = 1{\cdot}0$, (c) $H/B = 1{\cdot}5$.

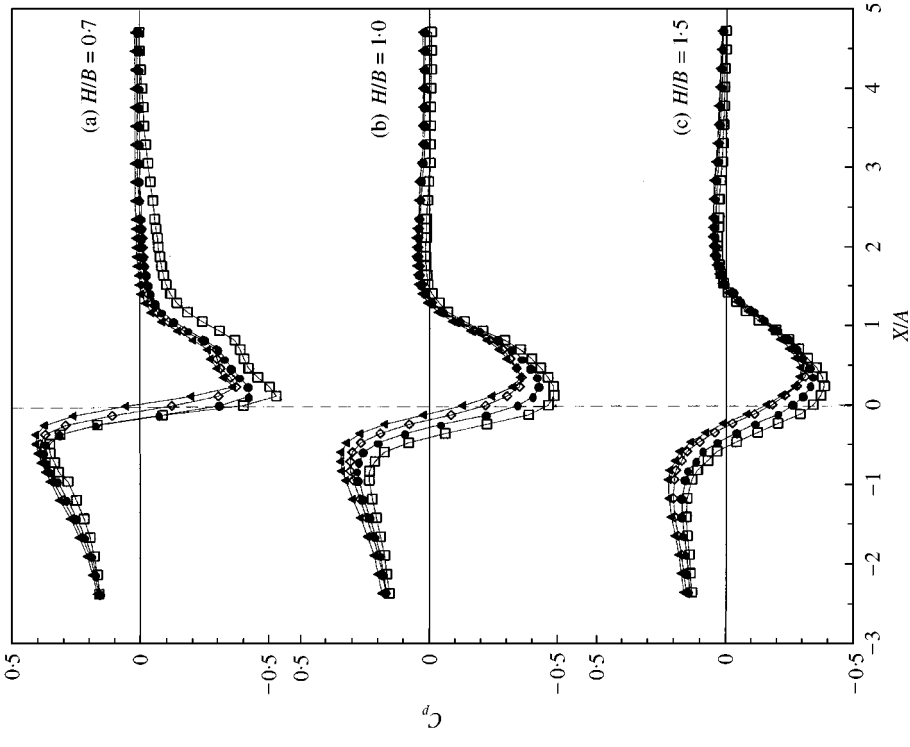

Figure 7. Surface pressure distributions on the flat plate at positive angles of attack: □, $\alpha = 0$; ●, $\alpha = 5°$; ◇, $\alpha = 10°$; ▲, $\alpha = 15°$. (a) $H/B = 0{\cdot}7$, (b) $H/B = 1{\cdot}0$, (c) $H/B = 1{\cdot}5$.

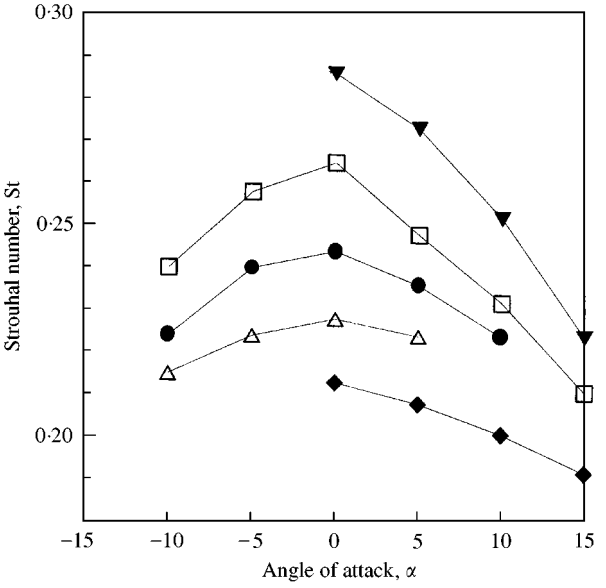

Figure 9. Variations of the Strouhal number in terms of angle of attack: ▼, at uniform flow; △, $H/B = 1{\cdot}0$; ●, $H/B = 1{\cdot}5$; □, $H/B = 2{\cdot}5$; ◆, Modi & Wiland (1990).

Strouhal number decreases as the angle of attack varies. This tendency is in good agreement with previous studies carried out on uniform flow (Modi & Wiland 1970; Ota *et al.* 1987), although the values of the Strouhal number are different due to the difference in the cylinder axes ratio.

As the gap ratio between the cylinder and plate decreases, the Strouhal number decreases regardless of the angle of attack. At the gap ratio of $H/B = 0{\cdot}7$, which is less than the critical gap ratio, we cannot see regular vortex shedding at any angle of attack. In previous studies (Bearman & Zdravkovich 1978; Lei *et al.* 1999; Choi & Lee 2000), the critical gap ratio at which regular vortices start to shed was determined. In this study, we can see the existence of a critical angle of attack in terms of the gap ratio. At negative angles of attack, the influence of the gap ratio on the critical angle of attack becomes larger than that for positive angles of attack.

Figure 10 shows the streamwise mean velocity and turbulence intensity profiles with respect to the angle of attack. Here, the solid line represents the velocity profile measured at the same location without the elliptic cylinder and the chain-dotted line indicates the center location of the elliptic cylinder. The vertical length scale is nondimensionalized using the boundary layer thickness at $X = 0{\cdot}0$ ($\delta_0 = 75$ mm). From the velocity profiles measured at gap ratio of $H/B = 1{\cdot}5$, the effect of the flow interaction between the boundary layer near the wall and the cylinder wake can be observed. For gap ratios less than $H/B = 1{\cdot}5$, we cannot observe the effect of the flow interaction. This is caused by the abrupt merging of the boundary layer near the wall and the cylinder wake. Similar results were observed in the work of Choi & Lee (2000) in which the ground effect of an elliptic cylinder was tested for a zero angle of attack.

Regardless of the angle of attack, the region of velocity deficit forms behind the cylinder, and the streamwise velocity profile near the ground plate approaches that of the boundary layer due to the high-speed gap flow. However, as the flow travels downstream, the wake behind the cylinder spreads out toward the wall region. Therefore, the velocity profiles have much smaller values than those in a boundary layer without a cylinder, due to the merging of the boundary layer near the wall and the cylinder wake.

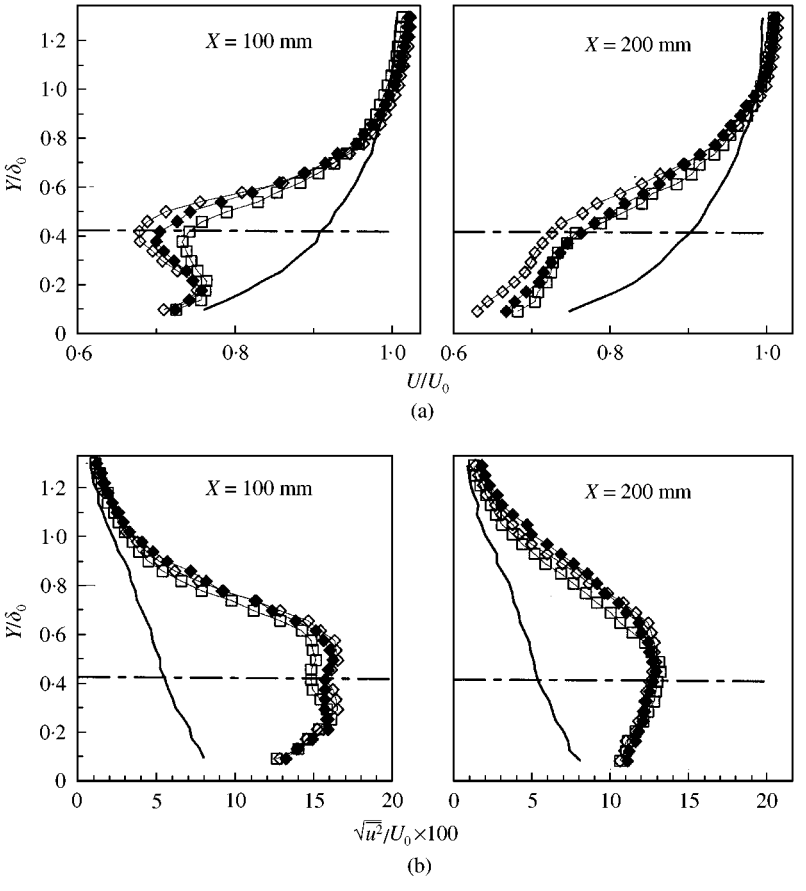

Figure 10. (a) Streamwise mean velocity and (b) turbulence intensity profiles at $H/B = 1{\cdot}5$. ◇, $\alpha = -15^{\circ}$; □, $\alpha = 0^{\circ}$; ◆, $\alpha = 15^{\circ}$.

As the angle of attack of the elliptic cylinder varies, the velocity deficit behind the cylinder also increases. The velocity deficit for a negative angle of attack becomes larger than for the same positive angle of attack. As the flow travels downstream ($X = 200$ mm), the velocity profile for the positive angle of attack ($\alpha = 15^{\circ}$) becomes similar to that of the zero angle of attack ($\alpha = 0^{\circ}$) case. On the other hand, the streamwise velocity profile at a negative angle of attack ($\alpha = -15^{\circ}$) has smaller values than in the case at the zero angle of attack. These results indicate that the merging of the separated wall shear layer from the flat plate and the lower shear layer of the cylinder wake becomes stronger at negative angles of attack than at positive ones. This is caused by the shift of the separation position on the lower surface of the elliptic cylinder. At negative angles of attack, the flow separation on the lower surface of the cylinder occurs near the front of the cylinder, whereas it appears near the rear of the cylinder for positive angles of attack. These flow characteristics are also observed in the flow visualization and the surface pressure distributions along the flat plate.

The turbulence intensity profiles at $X = 100$ mm have double peaks, which are peculiar in the near wake behind a symmetric bluff body located in a uniform flow. By turning the elliptic cylinder to generate an angle of attack, the magnitude of the turbulence intensity increases slightly in the central region of the wake. As the flow travels downstream, the turbulence intensity profiles become similar in shape, irrespective of the angle of attack. The

double peaks at $X = 100$ mm merge to form a single peak and the magnitude of the turbulence intensity decreases.

4. CONCLUSION

The flow characteristics around an elliptic cylinder with axis ratio of AR = 2 located near a flat plate were investigated experimentally. Various angles of attack of the cylinder were considered in order to study the interaction between the cylinder wake and the boundary layer.

As the angle of attack varies, the location of the peak pressure on the windward cylinder surface moves towards the rear edge of the cylinder, while that of the leeward surface moves toward the front edge of the cylinder. At positive angles of attack, the location of the minimum surface pressure on the flat plate moves downstream slightly, whereas it moves upstream for negative angles of attack.

With varying angles of attack, the vortex-shedding frequency gradually decreases and a critical angle of attack can be defined in terms of the gap ratio. At negative angles of attack, the boundary layer near the wall becomes disturbed more than for positive angles of attack. This shows that the merging of the separated wall shear layer from the boundary layer and the lower shear layer of the cylinder wake becomes stronger at negative angles of attack than at positive ones.

ACKNOWLEDGEMENTS

This work was supported by POSTECH and the National Research Laboratory Program of the Ministry of Science and Technology, Korea.

REFERENCES

BEARMAN, P. W. & ZDRAVKOVICH, M. M. 1978 Flow around a circular cylinder near a plane boundary. *Journal of Fluid Mechanics* **89,** 33–47.

CHOI, J. H. & LEE, S. J. 2000 Ground effect on flow around an elliptic cylinder in a turbulent boundary layer. *Journal of Fluids and Structures* **14,** 697–709.

LEI, C., CHENG, K. & KAVANAGH, K. 1999 Re-examination of the effect of a plane boundary on force and vortex shedding of a circular cylinder. *Journal of Wind Engineering and Industrial Aerodynamics* **80,** 263–286.

MARUMO, E., SUZUKI, K. & SATO, T. 1978 A turbulent boundary layer disturbed by a cylinder. *Journal of Fluid Mechanics* **87,** 121–141.

MASKELL, E. C. 1963 A theory of the blockage effects on bluff bodies and stalled wings in a closed wind tunnel. ARC Report and Memorandum No. 3400.

MODI, V. J. & WILAND, E. 1970 Unsteady aerodynamics of stationary elliptic cylinders in subcritical flow. *AIAA Journal* **8,** 1814–1821.

MODI, V. J. & DIKSHIT, A. K. 1975 Near wakes of elliptic cylinders in subcritical flow. *AIAA Journal* **13,** 490–497.

OTA, T., NISHIYAMA, H. & TAOKA, Y. 1984 Heat transfer and flow around an elliptic cylinder. *International Journal of Heat and Mass Transfer* **27,** 1771–1779.

OTA, T., NISHIYAMA, H. & TAOKA, Y. 1987 Flow around an elliptic cylinder in the critical Reynolds number regime. *ASME Journal of Fluids Engineering* **109,** 149–155.

RANZENBACH, R. & BARLOW, J. B. 1994 Two-dimensional airfoil in ground effect, an experimental and computational study. SAE 942509, 241–249.

ZHOU, M. D. & SQUIRE, L. C. 1985 The interaction of a wake with a turbulent boundary layer. *Aeronautical Journal* **89,** 72–81.